Journal of Materials Chemistry C

Semi-Transparent Low-Donor Content Organic Solar Cells Employing Cyclopentadithiophene-Based Conjugated Molecules

Journal:	*Journal of Materials Chemistry C*
Manuscript ID	TC-ART-06-2018-002863.R1
Article Type:	Paper
Date Submitted by the Author:	15-Aug-2018
Complete List of Authors:	Lee, Jungho; Ulsan National Institute of Science and Technology, ; Ulsan National Institute of Science and Technology, Interdisciplinary School of Green Energy Hernandez, Jeff; Georgia Institute of Technology, Chemistry& Biochemistry Pelse, Ian; Georgia Institute of Technology, Chemistryand Biochemistry, Materials Science and Engineering Reynolds, John; Georgia Institute of Technology, Chemistryand Biochemistry, Materials Science and Engineering Yang, Changduk; Ulsan National Institute of Science and Technology, Interdisciplinary School of Green Energy

Journal Name

ARTICLE

Semi-Transparent Low-Donor Content Organic Solar Cells Employing Cyclopentadithiophene-Based Conjugated Molecules

Jungho Lee[a,†], Jeff L. Hernandez[b,†], Ian Pelse[b], John R. Reynolds[b]*, Changduk Yang[a]*

Received 00th January 20xx,
Accepted 00th January 20xx

DOI: 10.1039/x0xx00000x

www.rsc.org/

Considering the facile synthesis of the cyclopentadithiophene (CPDT) building block, this study aims to synthesize and characterize two donor-acceptor type conjugated molecules, 2EH-CPDT(FBTTh$_2$)$_2$ and 5EN-CPDT(FBTTh$_2$)$_2$, with different branching points from the backbone. It was found that the branching point variation strategy slightly tunes the optical and electrochemical properties of the resulting conjugated molecule films owing to the difference between their intermolecular packing. When used as a donor material in PC$_{71}$BM-based organic solar cells (OSCs), the power conversion efficiency of 2EH-CPDT(FBTTh$_2$)$_2$ is twice that of the ones processed using 5EN-CPDT(FBTTh$_2$)$_2$. Interestingly, with no post treatments, OSCs were optimized with especially low-donor content within the active layer (donor:acceptor weight ratio = 1:9), which allows construction of a highly transparent film with a visible transmittance over 50%, showing a potential for application in integrated photovoltaics.

Introduction

Polymer-based organic solar cells (OSCs) have attracted significant attention in academia and industry owing to their potential value in the global solar energy market.[1-3] Recent advancements that have combined narrow band gap donor-acceptor polymer donors with soluble acceptors in a bulk heterojunction architecture have led to power conversion efficiency (PCE) values over 10%.[4-9] Recently, OSCs based on conjugated molecules have emerged as an alternative for the polymer counterparts owing to their well-defined structures without batch-to-batch variations, easy control of energy levels by designing a chemical structure, and relatively simple synthesis and purification.[10-12] One of the most successful OSC conjugated molecular skeletons can be described as containing a central donor core flanked by acceptor units and terminated with π-conjugated end-capping groups.[13-15]

Cyclopentadithiophene (CPDT), a fused ring bithiophene derivative, has attracted significant attention as a donor block for the construction of state-of-the-art narrow band gap donor-acceptor polymer donors. This is due to its efficient electron-donating nature and high co-planarity with strong intermolecular π–π interactions, as well as its facile synthesis from a commercially available reagents and simple side-chain manipulation for solubility.[16, 17] In fact, the Si or Ge analogues (e.g., dithienosillole and dithienogermole building blocks) have been used for successful OSC molecular frameworks,[18-23] however they have tedious multiple synthetic routes and difficulty in tuning side-chains. Therefore, there is a vast library of CPDT-containing polymers reported in the field of organic electronics including OSCs and organic field-effect transistors. However, little attention has been paid toward the design of discrete CPDT-based conjugated molecules.[24, 25]

In this work, two conjugated molecules, 2EH-CPDT(FBTTh$_2$)$_2$ and 5EN-CPDT(FBTTh$_2$)$_2$, were designed and synthesized with 2-ethylhexyl and 5-ethylnonyl side chains on the CPDT core, respectively, where they are affixed by the external 5-fluorobenzo[*c*][1,2,5]thiadiazole (FBT) and bithiophene moieties. While optimizing the OSCs, a surprisingly low 2EH-CPDT(FBTTh$_2$)$_2$:PC$_{71}$BM weight ratio of 1:9 was found to provide the highest performance, yielding an average PCE of 3.2%, which lead to active materials that are transparent across the visible spectrum. We believe that this study contributes toward a better understanding of the structure–property relationships in conjugated molecule-based OSCs and facilitates the design of new compounds for advanced high-performance transparent and semi-transparent photovoltaic devices.

Results and Discussion

The synthesis of (2EH-CPDT(FBTTh$_2$)$_2$ and 5EN-CPDT(FBTTh$_2$)$_2$) was carried out via a series of Migita–Kosugi–Stille cross-coupling reactions. The synthetic routes and structures are shown in Scheme 1, and the detailed procedures and spectroscopic characterization are given in the Experimental section.

[a] *Department of Energy Engineering, School of Energy and Chemical Engineering, Perovtronics Research Center, Low Dimensional Carbon Materials Center, Ulsan National Institute of Science and Technology (UNIST), 50 UNIST-gil, Ulju-gun, Ulsan 44919, South Korea. *Email: yang@unist.ac.kr*

[b] *School of Chemistry and Biochemistry, School of Materials Science and Engineering, Center for Organic Photonics and Electronics, Georgia Tech Polymer Network, Georgia Institute of Technology, Atlanta, Georgia 30332, United States. *Email: reynolds@chemistry.gatech.edu.*

† These authors contributed to the work equally.

Electronic Supplementary Information (ESI) available: ^{1}H NMR spectra, UV-Vis absorption spectra, DFT calculated geometry, OSCs characteristics and 1d GIWAXS line cut. See DOI: 10.1039/x0xx00000x

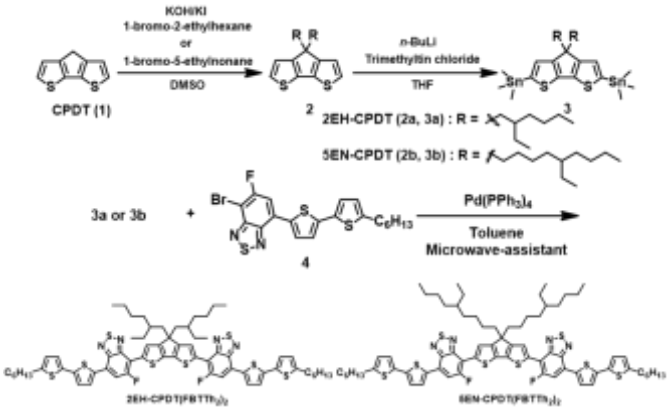

Scheme 1. Synthetic route for 2EH-CPDT(FBTTh$_2$)$_2$ and 5EN-CPDT(FBTTh$_2$)$_2$

The initial step during the synthesis involves a dialkylation onto the bridging methylene group of the CPDT core under basic conditions (KOH/KI). The 5-ethylnonyl-bromide was obtained by the synthetic sequences: coupling reaction of an alkyl halide with a Grignard reagent, hydroboration-oxidation, and bromination.[26] Additionally, the different reactivities of the two bromide functionalities in 4,7-dibromo-5-fluorobenzo[*c*][1,2,5]thiadiazole enabled access to the desired regioisomers where the two fluorine atoms are in a symmetric proximal/proximal configuration with respect to the central CPDT core.[18-22] Both products exhibit high solubility in most organic solvents and were structurally characterized using elemental analysis, NMR solution spectroscopy, and mass spectrometry.

Fig. 1a depicts the normalized UV-vis absorbance spectra of neat 2EH-CPDT(FBTTh$_2$)$_2$ and 5EN-CPDT(FBTTh$_2$)$_2$ in chloroform solution and thin film. Both 2EH-CPDT(FBTTh$_2$)$_2$ and 5EN-CPDT(FBTTh$_2$)$_2$ display dual absorption bands with distinct high and low energy bands attributed to localized π–π* and internal charge transfer transitions, respectively.[15, 18] Such absorption profiles are typically possessed by donor-acceptor type π-conjugated molecules. Their solution absorption spectra reveal a remarkable similarity, while a red shift of both absorption onset (λ_{onset}) and maximum (λ_{max}) in the film absorption spectra for 5EN-CPDT(FBTTh$_2$)$_2$ relative to 2EH-CPDT(FBTTh$_2$)$_2$ is observed. The optical band gap is reduced by 0.10 eV for 5EN-CPDT(FBTTh$_2$)$_2$ in comparison with that of 2EH-CPDT(FBTTh$_2$)$_2$. A rational explanation for this observation is greater molecular ordering of 5EN-CPDT(FBTTh$_2$)$_2$ in the solid state, which results in an improved inter-chromophore electronic coupling. This notion is consistent with the literature findings where moving the alkyl chain branching point away from conjugated backbones potentially allows the backbones to come closer and facilitates charge transport through intermolecular contact.[27-29] The highest occupied molecular orbital (HOMO) and lowest unoccupied molecular orbital (LUMO) energies of the conjugated molecules were determined from thin film cyclic voltammetry (CV) measurements, showing quasi-reversible oxidation and non-reversible reduction waves (Fig. 1b). The LUMO levels (−3.54 to −3.56 eV) are nearly identical for both molecules, while the HOMO level (−5.10 eV) for 5EN-CPDT(FBTTh$_2$)$_2$ is 0.15 eV higher than that of 2EH-CPDT(FBTTh$_2$)$_2$ (−5.25 eV). Furthermore, we also measured the ultraviolet photoelectron spectra (UPS) of the two material films, respectively (Fig. S4). The UPS-derived HOMO levels showed a similar trend and agreed with the CV results. From these CV and UPS results, we can conclude that the oxidation can be more facile and readily accommodated by the closer backbone packing induced by moving the alkyl branch site away from the CPDT backbone. Density functional theory calculations were also performed at the B3LYP/6-31G level using Gaussian 09. For computational simplicity, the 2-ethylhexyl and 5-ethylnonyl chains on the CPDT core were replaced with 2-methylpropyl and

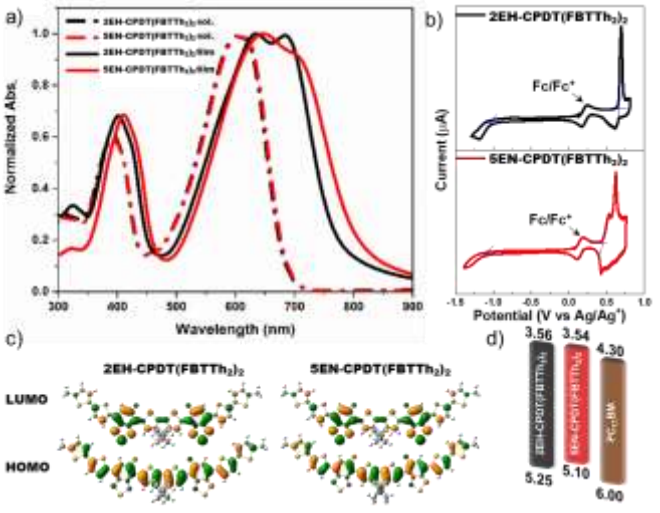

Fig. 1. a) Normalized UV-Vis absorption spectra of 2EH-CPDT(FBTTh$_2$)$_2$ and 5EN-CPDT(FBTTh$_2$)$_2$ in chloroform solution (dashed-dot line) and film (solid line). b) Cyclic voltammograms of 2EH-CPDT(FBTTh$_2$)$_2$ and 5EN-CPDT(FBTTh$_2$)$_2$ films with a ferrocene/ferrocenium couple (Fc/Fc+) as an internal standard. c) DFT calculated HOMO/LUMO geometry (top view) of 2EH-CPDT(FBTTh$_2$)$_2$ and 5EN-CPDT(FBTTh$_2$)$_2$. d) Energy diagrams of 2EH-CPDT(FBTTh$_2$)$_2$, 5EN-CPDT(FBTTh$_2$)$_2$ and PC$_{71}$BM.

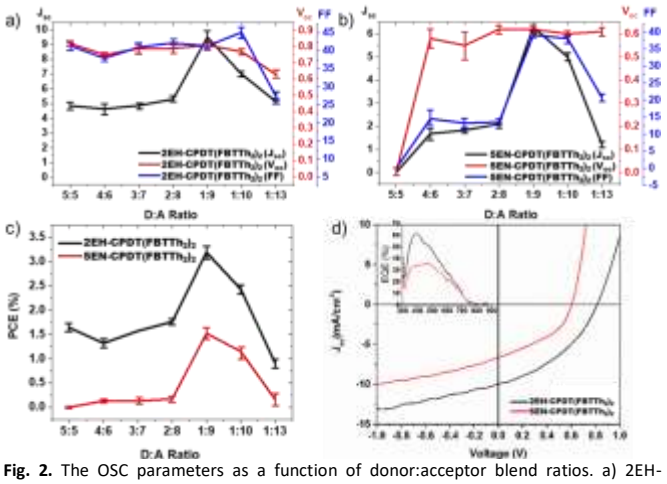

Fig. 2. The OSC parameters as a function of donor:acceptor blend ratios. a) 2EH-CPDT(FBTTh$_2$)$_2$ and b) 5EN-CPDT(FBTTh$_2$)$_2$ with PC$_{71}$BM. c) The PCE as a function of D:A ratio for both 2EH-CPDT(FBTTh$_2$)$_2$ and 5EN-CPDT(FBTTh$_2$)$_2$ with PC$_{71}$BM. d) *J*-*V* curves of optimized solar cells composed of 2EH-CPDT(FBTTh$_2$)$_2$:PC$_{71}$BM (black line) and 5EN-CPDT(FBTTh$_2$)$_2$:PC$_{71}$BM (red line) under AM 1.5G irradiation at 100 mW cm^{-2}.

Table 1. The optimized OSC results of 2EH-CPDT(FBTTh$_2$)$_2$ and 5EN-CPDT(FBTTh$_2$)$_2$ under AM1.5G illumination at 100 mW cm^{-2}.[a]

	J_{SC} (mA cm^{-2})	V_{OC} (V)	FF (%)	PCE (%)
2EH-CPDT(FBTTh$_2$)$_2$	9.5 ± 0.6	0.81 ± 0.01	41.4 ± 3.1	3.2 ± 0.2
5EN-CPDT(FBTTh$_2$)$_2$	6.3 ± 0.3	0.62 ± 0.02	39.1 ± 1.1	1.5 ± 0.1

[a] Average values of each parameter are gained over 6 devices.

5-methylhexyl units, and the terminal hexyl chains were changed to methyl groups. Both the models displayed almost identical molecular geometries and distributions of the HOMO and LUMO energies (Fig. 1c and Fig. S5).

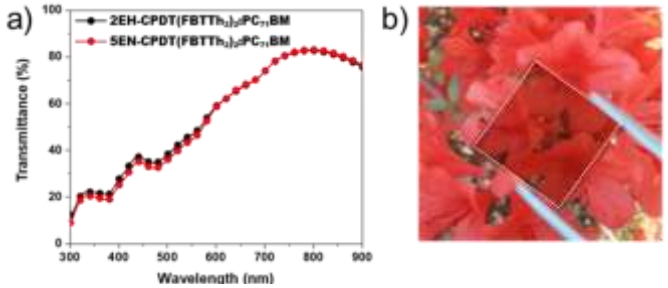

Fig. 3. a) The transmittance spectra of blend films with 1:9 weight ratio of 2EH-CPDT($FBTTh_2$)$_2$:$PC_{71}BM$ and 5EN-CPDT($FBTTh_2$)$_2$:$PC_{71}BM$. b) photograph of a film composed of 1:9 weight ratio of 2EH-CPDT($FBTTh_2$)$_2$:$PC_{71}BM$.

The photovoltaic properties of the donor molecules were evaluated in a conventional BHJ configuration (ITO/PEDOT:PSS/donor:(6,6)-phenyl-C_{71}-butyric acid methyl ester ($PC_{71}BM$) /Ca/Al) under inert atmosphere. The detailed procedures for the device fabrication are described in the Experimental section. We carefully optimized the OSC performance via controlling the donor:acceptor blend ratio within the active layer. Fig. 2a–c show the short circuit current density (J_{SC}), open circuit voltage (V_{OC}), fill factor (FF), and PCE as a function of the donor:acceptor weight ratio for 2EH-CPDT($FBTTh_2$)$_2$ and 5EN-CPDT($FBTTh_2$)$_2$ OSCs. The best performance was found with a donor:acceptor ratio of 1:9, which gave the highest J_{SC}, V_{OC}, and FF values among the tested systems. Although the PCE values in the proposed study are lower in comparison with the ones reported in recent articles, it is worth noting that both donor molecules show the best-performing OSCs with extremely low-donor content in the active layer, which, to the best of our knowledge, is rarely seen for other conjugated donor materials.[15, 18, 30-32] Interestingly, thermal and solvent-additive (1,8-diiodooctane) treatments decreased the device performance (Table S1, SI) and the devices, therefore, functioned best without such post processing treatments.[13, 31, 33-36] Fig. 2d shows the current density versus voltage (J–V) characteristics and the corresponding external quantum efficiencies (EQE) for the best-performing OSCs (donor:acceptor ratio of 1:9), and the photovoltaic parameters are detailed in Table 1 (see Table S2 for the complete device data as a function of donor:acceptor ratio). The 2EH-CPDT($FBTTh_2$)$_2$-based devices without any post treatments demonstrated an average PCE of 3.2%, which was more than twice than that of those based on 5EN-CPDT($FBTTh_2$)$_2$. The enhancement in PCE is mainly due to the improved J_{SC} and V_{OC}. While the slightly deeper-lying HOMO of 2EH-CPDT($FBTTh_2$)$_2$ does support the improvement in V_{OC}, we believe that there is still scatter in the data due to the other factors. In addition, it is also clear that, in comparison to devices based on 5EN-CPDT($FBTTh_2$), 2EH-CPDT($FBTTh_2$)-based devices show higher photo-conversion efficiency in the wavelength range from 300 to 750 nm, with the highest monochromatic EQE value over 60% at around 400 nm. A low donor OSC is beneficial because due to strong PCBM absorption at short wavelengths, the active layer can be made to be highly transparent; the optimized 2EH-CPDT($FBTTh_2$): $PC_{71}BM$ film displays over 65% transparency at long wavelengths beyond 650 nm and its average visible transmittance (AVT) calculated from the whole visible region (370−740 nm) is 50.4% (Fig. 3a).[37] To demonstrate the proposed application of this type of OSC, Fig. 3b shows an image of this optimized and nearly transparent film with the flowers behind clearly visible.

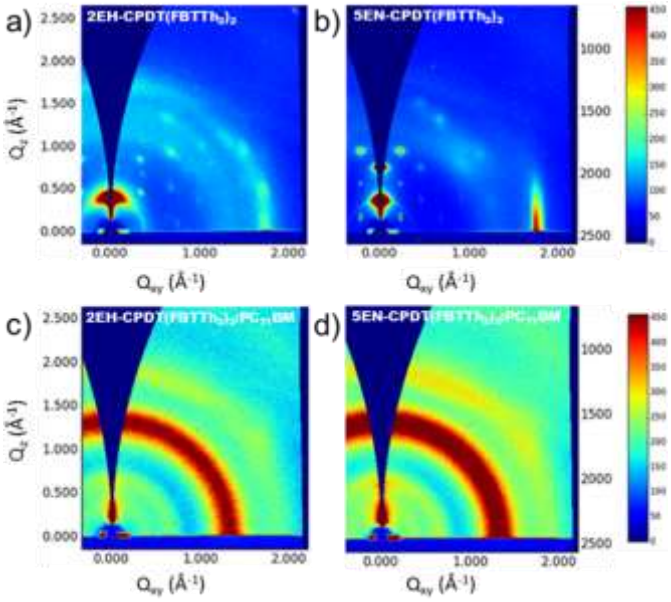

Fig. 4. 2D GIWAXS images of films composed of a) 2EH-CPDT($FBTTh_2$)$_2$, b) 5EN-CPDT($FBTTh_2$)$_2$, c) 2EH-CPDT($FBTTh_2$)$_2$:$PC_{71}BM$ (1:9) and d) 5EN-CPDT($FBTTh_2$)$_2$:$PC_{71}BM$ (1:9).

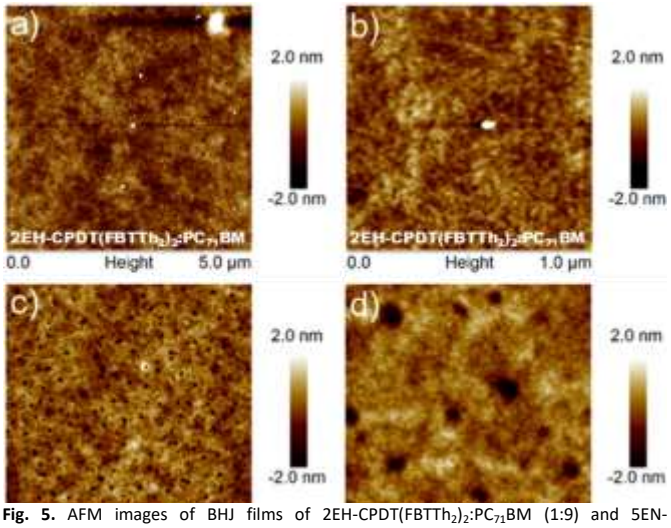

Fig. 5. AFM images of BHJ films of 2EH-CPDT($FBTTh_2$)$_2$:$PC_{71}BM$ (1:9) and 5EN-CPDT($FBTTh_2$)$_2$:$PC_{71}BM$ (1:9), taken a) and c) at 5 by 5 μm, b) and d) at 1 by 1 μm.

To understand the texture and molecular packing of the active layer morphology, grazing-incidence wide-angle x-ray scattering (GIWAXS) was collected for the neat and optimized blend films, as shown in Fig. 4. Their corresponding 1d line cuts in the q_z and q_{xy} directions are shown in Fig. S6, and crystallographic parameters are summarized in Table S3. In addition to the observation of many diffraction spots induced by multiple degrees of crystalline order, both neat films exhibited preferential edge-on π-stacking with respect to the substrate

with the evidence of strong (100) lamellar peak along q_z and (010) π–π peak along the q_{xy}. In comparison with 2EH-CPDT(FBTTh$_2$)$_2$, the neat 5EN-CPDT(FBTTh$_2$)$_2$ film showed more intense diffraction peaks, a strong enhancement of higher-order lamellar peaks, and a higher crystalline correlation length (CCL_{010}), which was determined using the Scherrer relation (7.7 nm for 2EH-CPDT(FBTTh$_2$)$_2$ vs. 16.9 nm for 5EN-CPDT(FBTTh$_2$)$_2$).[38] These observations suggest a greater extent of order and packing within 5EN-CPDT(FBTTh$_2$)$_2$, which is consistent with the UV-vis absorption results above.

On the contrary, for both BHJ films, there were scarcely any distinct diffraction peaks in both the qz and qxy directions, except for a symmetric circle at ~1.38 Å−1 corresponding to the intramolecular PC71BM distances. This signifies that the donor conjugated molecules are just dispersed into the PC71BM matrix without properly forming crystalline structures, which is most likely due to their very low content in the blend system. The amorphous and featureless textures of both the blend films are further supported by their atomic force microscopy (AFM) images where they have very fine and smooth surfaces with a small root-mean-square roughness (below 1 nm) (Fig. 5). It is noteworthy that 5EN-CPDT(FBTTh2)2 blend showed small indents with some pinholes, failing to achieve high film quality, which could be one of the reasons for their lower performance.

Conclusion

In this study, we synthesized two novel discrete conjugated molecules, (2EH-CPDT (FBTTh$_2$)$_2$ and 5EN-CPDT(FBTTh$_2$)$_2$), based on an alternating donor-acceptor architecture for OSC applications by utilizing the easily accessible CPDT building core and modifying the branching position of the side-chains. With a branch point shifted away from the CPDT backbone, 5EN-CPDT(FBTTh$_2$)$_2$ showed a red-shifted absorption spectrum in film and a higher-lying HOMO level with respect to 2EH-CPDT(FBTTh$_2$)$_2$. The best OSC based on 2EH-CPDT(FBTTh$_2$)$_2$:$PC_{71}BM$ without additional post processing exhibited more than 2-fold higher average PCE value than that of the 5EN-CPDT(FBTTh$_2$)$_2$-based OSC. Interestingly, unlike other conjugated donor materials, the optimized OSCs in this study were determined to have an extremely low donor content within the active layer (donor:acceptor ratio of 1:9), which enabled the fabrication of a highly transparent film (a high AVT of 50.4%). These results indicate that CPDT-based molecules are effective for use in transparent and semitransparent OSCs.

Experimental sections

General Procedures and Methods: All starting materials were purchased from Aldrich and Acros and used without further purification. All solvents are ACS grade unless otherwise noted. ^{1}H NMR and ^{13}C NMR spectra were recorded on a VNMRS 400 MHz spectrophotometer using $CDCl_3$ as solvent and tetramethylsilane (TMS) as the internal standard. UV-Vis spectra were taken on Cary 5000 (Varian USA) spectrophotometer. Cyclic voltammetry (CV) measurements were performed on Solartron electrochemical station (METEK, Versa STAT3) with a three-electrode cell in a 0.1 M tetra-*n*-butylammonium hexafluorophosphate (*n*-Bu_4NPF_6) solution in acetonitrile at a scan rate of 100 mV/s at room temperature under argon. Ag/Ag^+ electrode, a platinum wire and a platinum electrode were used as the reference electrode, counter electrode, and working electrode, respectively. The Ag/Ag^+ reference electrode was calibrated using a ferrocene/ferrocenium redox couple as an external standard, whose oxidation potential is set at -4.8 eV with respect to zero vacuum level. The HOMO energy levels were obtained from the equation HOMO (eV) = - ($E_{(ox)}^{onset}$ - $E_{(ferrocene)}^{onset}$ + 4.8). The LUMO levels of polymers were obtained from the equation LUMO (eV) = - ($E_{(red)}^{onset} - E_{(ferrocene)}^{onset}$ + 4.8). AFM was collected using a Bruker Dimension Icon Atomic Force Microscope with an RTESP-150 probe in standard tapping mode.

4,4-bis(2-ethylhexyl)-2,6-bis(trimethylstannyl)-4H-cyclopenta[1,2-b:5,4-b′]dithiophene (3a): The 2a (1 g, 2.5 mmol) was dissolved in anhydrous THF (25ml) and kept at -78°C under nitrogen flow. Then, *n*-butyllithium (2.2ml, 5.5 mmol, 2.5M in hexane) was slowly added. Subsequently, after stirring at -78 °C for 1hr, a trimethyltin chloride solution (5.5ml, 5.5 mmol, 1.0M in THF) was added. The reaction mixture was then slowly warmed to room temperature and stirred overnight. The mixture was quenched by adding water and extracted with diethyl ether for 3 times. The organic layer was dried over anhydrous $MgSO_4$ and concentrated under reduced pressure. The final product was obtained by column chromatography (AlO_x, *n*-hexane contained 10% of trimethylamine) to give 3a (1.4g, 77%) as a pale yellow oil. ^{1}H NMR (400 MHz, $CDCl_3$, δ) 6.98 (m, 2H), 1.85 (m, 4H), 1.30 (m, 2H), 0.92 (m, 16H), 0.78 (t, 6H), 0.62 (t, 6H), 0.38 (m, 18H).

4,4-bis(5-ethylnonyl)-2,6-bis(trimethylstannyl)-4H-cyclopenta[1,2-b:5,4-b′]dithiophene (3b): The 3b was prepared by the same method as the synthesis of **3a**. The **2b** (1g, 2.1 mmol), *n*-butyllithium (1.8ml, 4.6 mmol, 2.5M in hexane) and a trimethyltin chloride solution (4.6ml, 4.6 mmol, 1.0M in THF) were used to give 3b (1.2g, 72%) as a pale yellow oil. ^{1}H NMR (400 MHz, $CDCl_3$,δ) 6.98 (s, 2H), 1.85 (m, 4H), 1.30 (m, 24H), 0.92 (m, 12H), 0.78 (t, 6H), 0.38 (m, 18H).

7,7′-(4,4-bis(2-ethylhexyl)-4H-cyclopenta[1,2-b:5,4-b′]dithiophene-2,6-diyl)bis(6-fluoro-4-(5′-hexyl-[2,2′-bithiophene]-5-yl)benzo[c][1,2,5]thiadiazole) (2EH-CPDT(FBTTh$_2$)$_2$): The **3a** (300mg, 0.41 mmol), **4** (397mg, 0.82 mmol) and $Pd(PPh_3)_4$ (10mg, 0.008 mmol) were dissolved in anhydrous toluene (10ml) under nitrogen flow. The reaction mixture was heated to 100°C for 1 minute, 125°C for 1 minute, 140°C for 10 minutes, and 160°C for 10 minutes in microwave reactor. The reaction mixture was evaporated under reduced pressure and purified by column chromatography using *n*-hexane/chloroform gradient in several times to give 2EH-CPDT(FBTTh$_2$)$_2$ (250mg, 50%) as a dark purple solid. ^{1}H NMR (400 MHz, $CDCl_3$,δ) 8.24 (t, 2H), 8.05 (m, 2H), 7.76 (d, 2H), 7.20 (d, 2H), 7.14(d, 2H), 6.74 (d, 2H), 2.83 (t, 4H), 2.07 (m, 4H), 1.71 (m, 4H), 1.25 (m, 12H) 1.10 (m, 18H), 0.91 (m, 6H,), 0.64 (m, 12 H); ^{13}C NMR (100 MHz, $CDCl_3$, δ) 158.88, 157.00, 153.15, 153.03, 149.64, 146.29, 140.76, 140.22, 136.00, 134.40, 133.87, 128.85,

125.00, 123.95, 123.76, 116.11, 115.81, 112.00, 54.03, 43.14, 35.25, 34.27, 31.59, 31.56, 30.25, 28.80, 28.53, 27.51, 22.87, 22.60, 14.11, 14.05, 10.72; Elemental Analysis Calc. for $C_{65}H_{72}F_2N_4S_8$ C, 64.85 H, 6.03 N, 4.65 S, 21.31; Found: C, 64.81 H, 5.86 N, 4.63 S, 21.31. MALDI-TOF-MS m/z: $[M]^+$ =1204.33; calcd, 1203.81.

7,7′-(4,4-Bis(5-ethylnonyl)-4H-cyclopenta[1,2-b:5,4-b′]dithiophene-2,6-diyl)bis(6-fluoro-4-(5′-hexyl-[2,2′-bithiophene]-5-yl)benzo[c][1,2,5]thiadiazole) (5EN-CPDT(FBTTh$_2$)$_2$): The **3b** (300mg, 0.37 mmol), **4** (356mg, 0.74 mmol) and $Pd(PPh_3)_4$ (8.5mg, 0.0074 mmol) were dissolved in anhydrous toluene (9ml) under nitrogen flow. The reaction mixture was heated to 100°C for 1 minute, 125°C for 1 minute, 140°C for 10 minutes, and 160°C for 10 minutes in microwave reactor. The reaction mixture was evaporated under reduced pressure and purified by column chromatography using *n*-hexane/chloroform gradient in several times to give 5EN-CPDT(FBTTh$_2$)$_2$ (230mg, 48%) as a dark purple solid. ^{1}H NMR (400 MHz, $CDCl_3$,δ) 8.24 (s, 2H), 8.03 (m, 2H), 7.74 (d, 2H), 7.18(d, 2H), 7.12(d, 2H), 6.74 (d, 2H), 2.83 (t, 4H), 2.04 (m, 4H), 1.71 (m, 4H), 1.34 (m, 28H) 1.13 (m, 14H), 0.80 (m, 6H,), 0.74 (m, 12H); ^{13}C NMR (100 MHz, $CDCl_3$,δ) 159.33, 157.00, 152.99, 152.92, 149.52, 146.22, 140.57, 140.16, 135.89, 134.45, 133.65, 128.79, 124.93, 124.35, 123.88, 115.88, 115.56, 111.81, 53.92, 38.85, 37.81, 33.13, 32.82, 31.63, 31.56, 30.27, 28.97, 28.87, 27.38, 25.85, 25.34, 23.15, 22.64, 14.18, 14.15, 10.90; Elemental Analysis Calc. for $C_{71}H_{84}F_2N_4S_8$ C, 66.21 H, 6.57 N, 4.35 S, 19.92; Found: C, 65.94 H, 6.65 N, 4.34 S, 19.94. MALDI-TOF-MS m/z: $[M]^+$ =1288.47; calcd, 1287.97.

GIWAXS measurements were carried out on beamline 11-3 at the Stanford Synchrotron Radiation Light source (SSRL) with the help of Dr. Chris Tassone. The beam was kept at an energy of 12.7 keV with an incidence angle of 0.13°. A LaB_6 standard sample was used to calibrate the instrument and the software WxDiff ver 1.20 was used to reduce the 2d scattering data into the corrected 1d integration plots (I vs q).[39] Neat films and bulk-heterojunction films were coated on top of PEDOT:PSS (Clevios P VP AI 4083)/Si.

OSC Device Fabrication: Pre-patterned indium tin oxide (ITO) was sonicated for 5 minutes each in a solution of sodium dodecyl sulfate (SDS) purchased from Sigma Aldrich in 18 MΩ water obtained from a Millipore Direct Q 3 UV system, then acetone, then isopropanol. The ITO was then UV-ozone cleaned for 10 minutes. PEDOT:PSS (Clevios P VP AI 4083) was filtered with a 13 mm 0.45 µm Nylon syringe, spun coat on cleaned ITO at 5000 rpm for 50 seconds, then dried on a 120°C hotplate in air for 10 minutes. Solutions of either 2EH-CPDT(FBTTh$_2$)$_2$ or 5EN-CPDT(FBTTh$_2$)$_2$ with $PC_{71}BM$ (15 mg mL^{-1} total solid concentration) was spun coated on the PEDOT:PSS/ITO at 800 rpm for 50 seconds in an Ar filled glovebox. Sequential deposition of 10 nm of Ca followed by 100 nm of Al were evaporated at a pressure of 10^{-5} mbar as the top electrodes. Devices were tested with a Newport ABB class solar simulator attached to a Kiethley 2410 SMU source meter for AM 1.5G measurements calibrated to 100 mW cm^{-2}. The device active area is 0.08 cm^2, which is defined by the overlapping area of the top and bottom electrode.

Acknowledgements

This work was supported by the Center for Advanced Soft-Electronics funded by the Ministry of Science and ICT as Global Frontier Project" (2012M3A6A5055225) and the Research Project Funded by U-K Brand (1.180043.01) of UNIST(Ulsan National Institute of Science & Technology). J.R.R. acknowledges the Office of Naval Research (N00014-17-1-2243 and N00014-16-1-2520) for funding of this work. J.L.H acknowledges the NSF NESAC IGERT (DGE-1069138) program for Traineeship support. I.P. was supported by the Department of Defense (DoD) through the National Defense Science & Engineering Graduate Fellowship (NDSEG) Program.

References

1. C. Wang, H. Dong, W. Hu, Y. Liu and D. Zhu, *Chem. Rev.*, 2011, **112**, 2208.
2. L. Lu, T. Zheng, Q. Wu, A. M. Schneider, D. Zhao and L. Yu, *Chem. Rev.*, 2015, **115**, 12666.
3. L. Dou, Y. Liu, Z. Hong, G. Li and Y. Yang, *Chem. Rev.*, 2015, **115**, 12633.
4. W. Zhao, D. Qian, S. Zhang, S. Li, O. Inganäs, F. Gao and J. Hou, *Adv. Mater.*, 2016, **28**, 4734.
5. L. Ye, S. Zhang, W. Zhao, H. Yao and J. Hou, *Chem. Mater.*, 2014, **26**, 3603.
6. Y. Liu, J. Zhao, Z. Li, C. Mu, W. Ma, H. Hu, K. Jiang, H. Lin, H. Ade and H. Yan, *Nat. Commun.*, 2014, **5**, 5293.
7. K.-G. Lim, M.-R. Choi and T.-W. Lee, *Mater. Today Energy*, 2017, **5**, 66.
8. H. Kim, J. Byun, S. H. Bae, T. Ahmed, J. X. Zhu, S. J. Kwon, Y. Lee, S. Y. Min, C. Wolf and H. K. Seo, *Adv. Energy Mater.*, 2016, **6**, 1600172.
9. K.-G. Lim, S. Ahn and T.-W. Lee, *J. Mater. Chem. C*, 2018, **6**, 2915.
10. S. S. Zade, N. Zamoshchik and M. Bendikov, *Acc. Chem. Res.*, 2010, **44**, 14.
11. C. Kim, J. Liu, J. Lin, A. B. Tamayo, B. Walker, G. Wu and T.-Q. Nguyen, *Chem. Mater.*, 2012, **24**, 1699.
12. Z. B. Henson, K. Müllen and G. C. Bazan, *Nat. Chem.*, 2012, **4**, 699.
13. K. Wang, R. Z. Liang, J. Wolf, Q. Saleem, M. Babics, P. Wucher, M. Abdelsamie, A. Amassian, M. R. Hansen and P. M. Beaujuge, *Adv. Funct. Mater.*, 2016, **26**, 7103.
14. A. Tang, C. Zhan and J. Yao, *Adv. Energy Mater.*, 2015, **5**, 1500059.
15. Y. Sun, G. C. Welch, W. L. Leong, C. J. Takacs, G. C. Bazan and A. J. Heeger, *Nat. Mater.*, 2012, **11**, 44.
16. Y. Yamashita, F. Hinkel, T. Marszalek, W. Zajaczkowski, W. Pisula, M. Baumgarten, H. Matsui, K. Müllen and J. Takeya, *Chem. Mater.*, 2016, **28**, 420.
17. F. Hinkel, T. Marszalek, W. Zajaczkowski, S. R. Puniredd, M. Baumgarten, W. Pisula and K. Müllen, *Chem. Mater.*, 2014, **26**, 4844.
18. M. Moon, B. Walker, J. Lee, S. Y. Park, H. Ahn, T. Kim, T. H. Lee, J. Heo, J. H. Seo, T. J. Shin, J. Y. Kim and C. Yang, *Adv. Energy Mater.*, 2015, **5**, 1402044.
19. T. S. Van Der Poll, J. A. Love, T. Q. Nguyen and G. C. Bazan, *Adv. Mater.*, 2012, **24**, 3646.
20. D. Han, T. Kumari, S. Jung, Y. An and C. Yang, *Sol. RRL*, 2018, **2**, 1800009.

21. B. Walker, D. Han, M. Moon, S. Y. Park, K.-H. Kim, J. Y. Kim and C. Yang, *ACS Appl. Mater. Interfaces*, 2017, **9**, 7091.
22. D. Han, J. Lee, S. M. Lee, J. H. Seo, S. H. Park and C. Yang, *Dyes Pigment.*, 2018, **155**, 7.
23. T. Kumari, M. Moon, S.-H. Kang and C. Yang, *Nano Energy*, 2016, **24**, 56.
24. M. Zhang, H. N. Tsao, W. Pisula, C. Yang, A. K. Mishra and K. Müllen, *J. Am. Chem. Soc.*, 2007, **129**, 3472.
25. Z. Li, S. W. Tsang, X. Du, L. Scoles, G. Robertson, Y. Zhang, F. Toll, Y. Tao, J. Lu and J. Ding, *Adv. Funct. Mater.*, 2011, **21**, 3331.
26. J. Lee, T. Marszalek, K. C. Lee, J. Kim, W. Pisula and C. Yang, *Macromol. Chem. Phys.*, 2015, **216**, 1244.
27. J. Mei, D. H. Kim, A. L. Ayzner, M. F. Toney and Z. Bao, *J. Am. Chem. Soc.*, 2011, **133**, 20130.
28. T. Lei, J. H. Dou and J. Pei, *Adv. Mater.*, 2012, **24**, 6457.
29. J. Lee, A.-R. Han, H. Yu, T. J. Shin, C. Yang and J. H. Oh, *J. Am. Chem. Soc.*, 2013, **135**, 9540.
30. J. L. Wang, Q. R. Yin, J. S. Miao, Z. Wu, Z. F. Chang, Y. Cao, R. B. Zhang, J. Y. Wang, H. B. Wu and Y. Cao, *Adv. Funct. Mater.*, 2015, **25**, 3514.
31. H. Wang, F. Liu, L. Bu, J. Gao, C. Wang, W. Wei and T. P. Russell, *Adv. Mater.*, 2013, **25**, 6519.
32. C. Cui, X. Guo, J. Min, B. Guo, X. Cheng, M. Zhang, C. J. Brabec and Y. Li, *Adv. Mater.*, 2015, **27**, 7469.
33. C. D. Wessendorf, G. L. Schulz, A. Mishra, P. Kar, I. Ata, M. Weidelener, M. Urdanpilleta, J. Hanisch, E. Mena-Osteritz and M. Lindén, *Adv. Energy Mater.*, 2014, **4**, 1400266.
34. J. L. Wang, F. Xiao, J. Yan, Z. Wu, K. K. Liu, Z. F. Chang, R. B. Zhang, H. Chen, H. B. Wu and Y. Cao, *Adv. Funct. Mater.*, 2016, **26**, 1803.
35. L. Li, L. Xiao, H. Qin, K. Gao, J. Peng, Y. Cao, F. Liu, T. P. Russell and X. Peng, *ACS Appl. Mater. Interfaces*, 2015, **7**, 21495.
36. D. Deng, Y. Zhang, L. Yuan, C. He, K. Lu and Z. Wei, *Adv. Energy Mater.*, 2014, **4**, 1400538.
37. K.-S. Chen, J.-F. Salinas, H.-L. Yip, L. Huo, J. Hou and A. K.-Y. Jen, *Energy Environ. Sci.*, 2012, **5**, 9551.
38. D.-M. Smilgies, *J. Appl. Crystallogr.*, 2009, **42**, 1030.
39. S. Mannsfeld, *Stanford Synchrotron Radiation Light-Source*, 2009.